Investigation of the Potential-Induced Aging Phenomenon of an Insulating Encapsulant for a Photovoltaic Module: From Electrical to Chemical Properties

Jiawei Zhang, Fan Xu, Xiaojing Chen, Chatchai Putson, Sombel Diaham, Qian Wang

Investigation on the potential induced aging phenomenon of insulating encapsulant for photovoltaic module: from electrical to chemical properties

Jiawei Zhang[a]*, Fan Xu[a], Xiaojing Chen[b], Chatchai Putson[c], Sombel Diaham[d], Qian Wang[a]

[a] *School of Electrical Engineering, Xi'an University of Technology, Xi'an, Shanxi 710048, China*

[b] *College of Physics and Electronic Engineering Information, Wenzhou University, Wenzhou, Zhejiang 325035, China*

[c] *Materials Physics Laboratory, Department of Physics, Faculty of Science, Prince of Songkla University (PSU), Songkhla 90112, Thailand*

[d] U*niversité de Toulouse, UPS, INPT, LAPLACE (Laboratoire Plasma et Conversion d'Energie), 118 route de Narbonne, F-31062 Toulouse cedex 9, France*

* Corresponding author: Jiawei Zhang

Email: jwzhang@xaut.edu.cn

Tel: +86(0) 29-82312002; Fax: +86(0) 29-82312002

ABSTRACT

We analyzed the degradation phenomenon and mechanism induced by electrical field of encapsulant layer for photovoltaic module. The discharge number and discharge energy were analyzed in terms of the phase-resolved partial discharge pattern, and the changes of functional group and crystallinity were investigated with regard to the infrared, Raman spectroscopy and differential scanning calorimetry. The calculated discharge energy reflected that the overall encapsulant layer has higher partial discharge (PD) resistance. Furthermore, the changes of functional group and crystallinity

demonstrated the influence of electrical field on the molecular structure. These results could provide reference on perfecting the corresponding testing standards for the encapsulant material and designing the encapsulant layer for photovoltaic module in deep space exploration in future investigation.

KEYWORD: Photovoltaic system, Electrical degradation, Encapsulant layer, discharge energy, Functional group, Crystallinity

1. Introduction

The rapid promotion of "carbon peaking and carbon neutralization" has accelerated the development of new energy system [1-3]. Considered the abundant reserves, solar energy obtains more attentions and gradually serves as the best substitute for mitigating the global energy crisis and greenhouse effect caused by the extensive burning of conventional fossil energy [4,5]. According to the World Energy Outlook (WEO), solar photovoltaic (PV) could increase to 740 TWh by the end of 2035 [6], which supplied human beings with considerable power to complete daily life and to accomplish industrial production. The degradation of encapsulant materials of PV modules is the main explanation driving the decrease of service life of solar energy systems. Thus, a large number of studies related to the aging properties of encapsulant materials were performed for the sake of providing paths to ameliorate the performance of PV systems after being subjected to temperature, damp heat (DH), ultraviolet irradiation (UV), salt mist and so on according to the IEC 61215 and IEC 61730. These factors can result in the failure and ageing of PV module, as shown in figure 1.

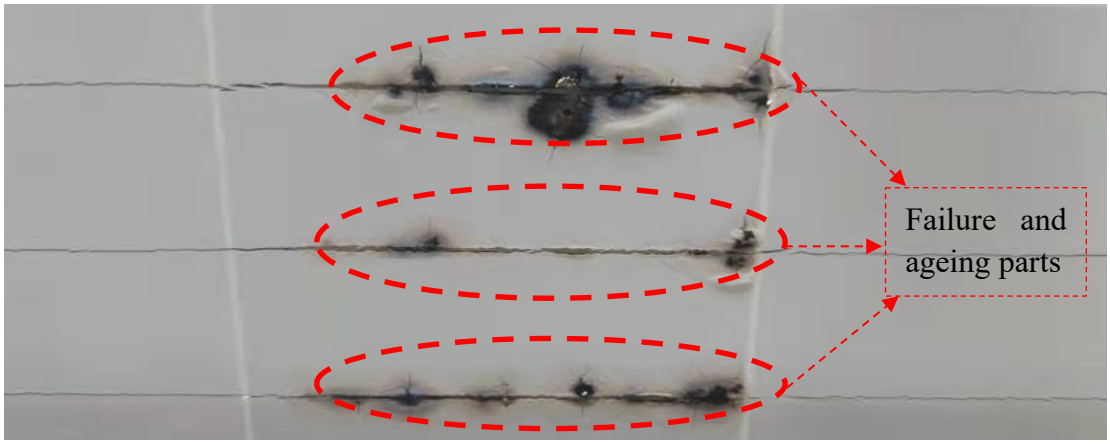

Figure 1. Insulating failure of PV module

Gagliardi M et al. [7] investigated the thermo-oxidative aging of ethyl vinyl acetate (EVA) encapsulant film by accelerating environmental tests and finite element model under different environmental conditions. After continuous optimization, the model could be used to predict EVA degradation and the service time of the PV module. However, the model only took into account the external macroscopic factors, micro factors such as energy and chemical changes need to be further study for better predicting polymer insulation degradation and the lifetime of the PV module. Adothu B et al. [8] studied thermoplastic polyolefin (TPO) replacing the EVA encapsulant used to package the advanced solar PV system. In his work, UV accelerated test and Raman spectra were performed to analyze the applicability of TPO encapsulant. The results indicated that the TPO could replace the EVA for packaging the PV system because of

the advantages of excellent transmittance, thermal property and mechanical performance. However, the electrical property of EVA film after UV exposure was ignored in his study. Therefore, it is necessary to explore electrical properties of TPO encapuslant. Liu F et al. [9] studied the EVA film subjected to different hours of UV exposure to investigate the physical degradation by visual inspection, scanning electron microscope (SEM) and chemical degradation by fourier transform infrared (FTIR) spectra. Nevertheless, as the encapsulant of PV system, the electrical properties should be worthy of attention. Zhang J W et al. [10] explored the aging properties of TPT (polyvinyl fluoride, PET, polyvinyl fluoride) and KPK (polyvinylidene fluoride, PET, polyvinylidene fluoride) backsheets caused by partial discharge (PD) and corona discharge. Moreover, the variation of surface roughness caused by the charge bombardment as well as the deposition of chemical groups was observed by atomic force microscope (AFM) images. He puts forward a significant method for researching the relationship between the service time of polymeric backsheet and electrical aging. But the discharge energy was not explored in his paper.

However, there are few investigations on the electrical performance of encapsulant material and the overall electrical performance of hot-melting encapsulant adhesive film on polyethylene terephthalate (PET) backsheet. Meanwhile, some studies [11,12] have proposed that PD event is one of the most common activities, resulting in the electrical failure or breakdown of the insulating system. PD event is one of the early indicators of insulation failure. Therefore, it is mandatory to perform PD test for exploring the electrical performance of encapsulant layer of PV system.

The polyolefin elastomer (POE) adhesive film used to package the bifacial glass modules mainly includes POE and new co-extrusive POE (EVA-POE-EVA) films. The POE film and EPE film are a type of thermoplastic rubber and thermosetting material respectively, performing its role by crosslinking reaction. Generally, the crosslinking reaction is performed by the lamination process from 130 ℃ to 160 ℃ in vacuum to cure film with other PV modules, which can package and seal the PV modules for a long time by the generation of covalent bonds between polymer molecular chains [13]. The POE is a kind of random copolymer, which mainly consists of octylene and ethylene. Firstly, the narrow distribution of relative molecular mass and the dense distribution of short branched chain decide that POE has excellent mechanical properties, which are attributed to higher elasticity, higher strength, higher elongation and better low temperature property. Secondly, POE molecular chain is saturated and contains fewer tertiary carbon atoms, which makes POE has excellent anti-ultraviolet and anti-heat aging properties. In addition, due to the application of metallocene catalysis technology, the position and dosage of copolymers are controllable, and the copolymers destroy the crystallization of ethylene, which lead to good elasticity and excellent light transmission of POE. The EVA-POE-EVA (EPE) film, merged the advantages of EVA and POE films, is the novel three-layer encapsulant material for bifacial glass modules. In order to better utilize the POE adhesive film for the advanced PV system, it is necessary to explore the performance of POE film, EPE film, the overall encapsulant layer of hot-melting POE on PET backsheet and the overall encapsulant layer of hot-melting EPE on PET backsheet from electrical perspective to chemical

perspective.

In order to evaluate the reliability and durability of insulating encapsulant for PV module, it is vital to perform PD test [14]. In this paper, at first, the PD tests of POE and EPE films were carried out for 2 h., and the overall encapsulant layer of hot-melting POE on PET backsheet, and the overall encapsulant layer of hot-melting EPE on PET backsheetwere carried out for 10 h. Subsequently, the variation of chemical group on the POE adhesive film was also by infrared and Raman spectra after PD. Meanwhile, the differential scanning calorimetry (DSC) were employed to analyze the crystallinity of the tested samples after PD. The results in this paper provide a more accurate approach to comprehensively evaluate the degradation degree and performance of the insulating encapsulant for solar energy systems and other insulating polymer in smart grid in the future investigation.

2. Experiment

Prior to the ageing test, the 0.79-mm-thick POE and 0.63-mm-thick EPE films were treated with anhydrous alcohol. Then, an ionizing air blower was employed to dry these samples and eliminate the deposited charge on the surface of POE and EPE films. Subsequently, the POE and EPE films, placed on 0.25-mm-thick PET, were subjected to 140 ℃ in vacuum to perform hot-melting process. After that, the thicknesses of the overall encapsulant layer of hot-melting POE and EPE on PET backsheet are around 0.83 mm and 0.80 mm. In order to explore the electrical ageing of POE films, EPE films, the overall encapsulant layer of hot-melting POE on PET backsheet and the overall encapsulant layer of hot-melting EPE on PET backsheet, the POE and EPE films, cut into 20 × 20 mm square, were placed in PD experimental platform to suffer from discharge for 2 h. Meanwhile, the overall encapsulant layer of hot-melting POE on PET backsheet and the overall encapsulant layer of hot-melting EPE on PET backsheet, cut into 20 × 20 mm square, were placed in PD experimental platform to suffer from discharge for 10 h. The partial discharge inception voltage (PDIV) was measured firstly; then the applied voltage should be set at 110% PDIV for simulating electrical degradation. The PD test platform mainly comprises an alternating current (AC) power source (EVERFINE GK10010, China), a high frequency current transformer (HFCT050, China), a boosting transformer (HNSC BK-1200, China), and a high voltage differential probe (PINTEK DP-100, China), which is shown in figure 2 in detail. The data transmission system is consisted of an oscilloscope (KEYSIGHT MSO-X 4104A, USA) and a computer. Subsequently, an infrared spectroscopy tester (THERMO SCIENTIFIC NICOLET iS20, USA) was employed to perform infrared spectroscopy tests in a closed environment. The total specimens were measured five times, and the measurements were averaged. Raman spectroscopy tests were carried out with a confocal Raman microscope (HORIBA HR EVOLUTION, France). In order to analyze the thermal characteristics of the POE and EPE adhesive films after PD, the differential scanning calorimetry (DSC) measurement of POE adhesive films was performed in a temperature range of 30-200 ℃ with the heating rate of 10 ℃/min by DSC tester (DSC Q2000, USA).

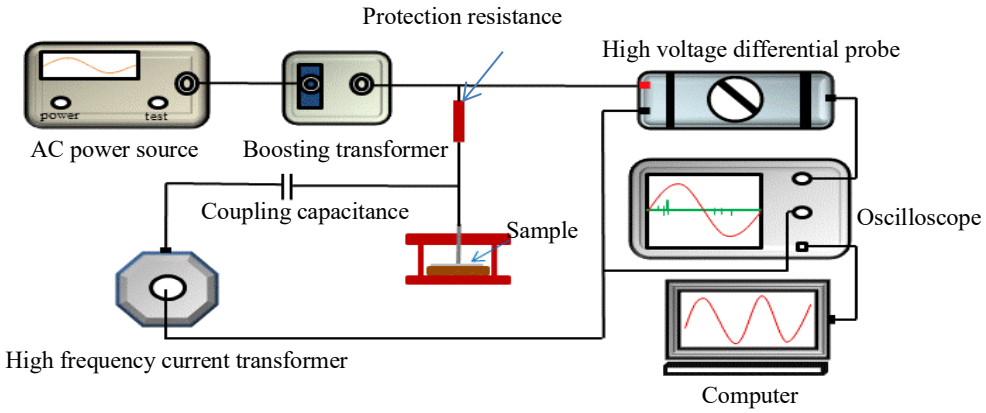

Figure 2. Schematic of the PD test platform

3. Results and Discussion

3.1 PD Activity Measurement

The phase-resolved partial discharge (PRPD) pattern is an effective diagnostic parameter employed for analyzing the electrical aging activity of polymer material. Figure 3 a-d shows the PRPDs of the POE films, the overall encapsulant layer of the hot-melting POE on PET backsheet, EPE films and the overall encapsulant layer of the hot-melting EPE on PET backsheet, respectively. The PDIVs of POE and EPE films are 2182V and 1636 V, and the PDIVs of the overall encapsulant layer of the hot-melting POE on PET backsheet, the overall encapsulant layer of the hot-melting EPE on PET backsheet are 2455 V and 1840 V, respectively. Those samples were subjected to electrically stressing at 110% of the PDIV for PD tests. As depicted in figure 3, it is obvious that PD events on all the samples occur at a phase angle of 0 to 90° and 180 to 270°. The drop off in field at the defects inside the above samples, induced by the opposite field polarity between the field caused by the stored space charge and the applied field after the occurrence of first discharge activity, is a large contributor to PD phenomenon appeared at a specific phase angle [15]. The PRPDs evidently appear two regions marked with red and black. The red parts are considered as regions where the PD activities frequently occur, whereas the black parts indicate those regions that the PD events infrequently appear. It is clear that the EPE film and the overall encapsulant layer of hot-melting EPE on PET backsheet have more number of PD events than that of POE film and the overall encapsulant layer of hot-melting POE on PET backsheet, respectively. In addition, it can be noticed that PD activity with more repetition rate displays lower discharge magnitude and shorter duration. On the contrary, PD activity with less repetition rate exhibits higher discharge magnitude as well as a noticeably longer duration. Compared with the POE film, the EPE film exhibits relative intensive PD activity, which could be attributed to the surface layer (EVA) with lower PD resistance than that POE film. Partial discharge inception fields confirm the above mentioned phenomenon alike. In addition, it can be found that the overall encapsulant layer of the hot-melting POE and EPE on PET backsheet show higher PD resistance than that of POE and EPE film. On the one hand, during hot-melting process, POE and EPE films can occur partial crosslinking, which connects each linear molecule to form

three-dimensional molecular structure. Crosslinking reaction not only improves its strength, heat resistance, but also improves its mechanical and chemical properties [16]. On the other hand, the hot-melting POE or EPE, PET have excellent insulation performance, which further improves the insulation performance of the overall encapsulant layer of the hot-melting POE and EPE on PET backsheet.

PD event is a kind of discharge activity when the applied electric field strength is enough to generate discharge event in partial insulation area, but specific discharge path is not formed in the discharge area. Partial discharge usually occurs in the internal defects of insulating materials or in the contact part between conductor and insulation. The electric field strength at defect is often greater than that of other parts, which is prone to occur PD at defect. Although PD generally does not cause the penetrating breakdown of insulation for a short time, it often causes the partial damage of dielectric. If PD exists for a long time, it can result in the initiation and growth of electrical tree leading to insulation failure or breakdown [17]. Specifically, the high energy electrons generated by partial discharge bombard the surface and internal defects of the material, which destroy the molecular bonds of the material and produce oxidation products, further aggravating the partial discharge. Finally, insulation failure or breakdown occur at defects of insulation material.

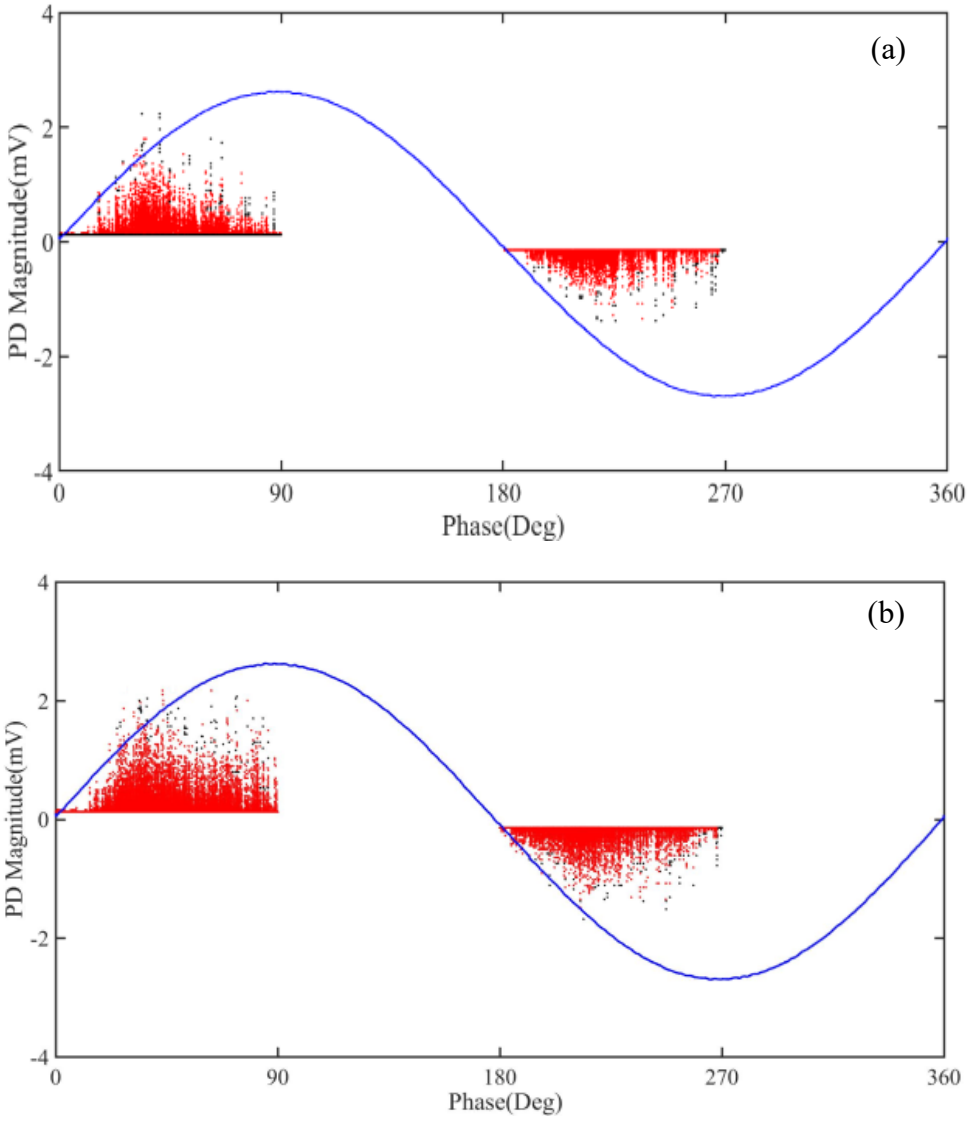

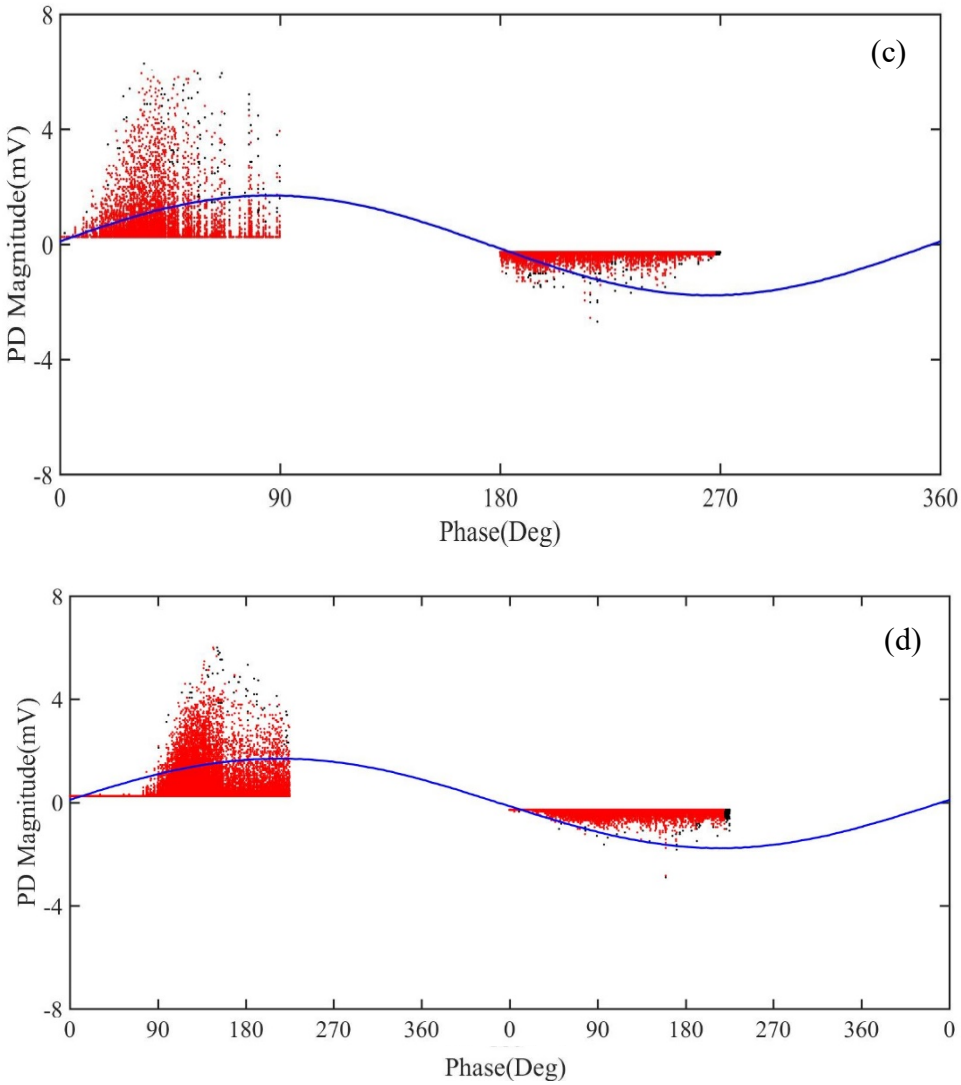

Figure 3. PRPD of POE film after PD 2 h (a), EPE film after PD 2 h (b), overall encapsulant of hot-melting POE on PET backsheet (c), overall encapsulant of hot-melting EPE on PET backsheet (d).

An initial seed electron could lead to electron avalanche, which is a critical precondition for the occurrence of a PD activity [15,17-23]. The number of initial seed electron has effect on the statistical characteristics of PD event, which includes the delay of initial partial discharge, frequency of the occurrence of PD activity, and the PRPD [15]. The main generation mechanism of initial seed electron is the surface process including field emission from cathode of conductors, detrapping of electron on the insulation surface or traps under low energy levels, electrons release induced by ionization processes, and the photo effect of the surface of insulating backsheet [20,21]. The generation rate of seed electron is mainly related to the applied voltage (applied filed), material conductivity and permittivity and so on.

Then, PD is induced by the increase of a local field triggered by the defects inside insulating material, which usually is ignited by a relatively higher applied voltage or

previous PD event [24,25]. During PD, chemical reactions and electron bombardment occur in defects of insulating materials, which leads to the enhancement of local electrical field and surface conductivity at defects. Consequently, it is more prone to generate a second discharge at the area of the previous PD, which could be induced by the increase of surface conductivity caused by PD [17]. As a result of PD event, the number of trap continuously raise as lengthening the applied voltage time, which makes more electrons deposit at defects. The deposited charge induced by PD results in the potential difference across the defects, and it is deemed that the deposited charge could generate more initial seed electrons.

With the continuous development of partial discharge, by-product attached to defects of insulating material increase constantly, which results in the increase of roughness at defects. Meanwhile, crystallization and chemical corrosion also occur in defects, which further leads to the change of electric field around the crystallization. The above mentioned changes could give rise to more obvious partial discharge at the defects, which results in the growth of electrical tree inside the material. Finally, the insulation material is broken down due to the continuous growth of electrical tree.

In order to evaluate the degradation degree of the solar energy systems, the discharge energy of POE adhesive films was calculated after PD test. Equation (1) is charge quantity (Q_i) during PD [26].

$$Q_i = \int_{t_2}^{t_1} I_i \, dt \tag{1}$$

Where I_i is instantaneous current for each PD pulse, t_1 and t_2 are the inception time and end time for each PD pulse, respectively.

Equation (2) describes PD energy [27].

$$W = \sum_i Q_i \cdot U_i \tag{2}$$

Where Q_i, U_i are the apparent charge and transient voltage for each PD pulse, respectively.

The discharge energies of POE film after PD 2 h is 6.7314×10^6 pJ, respectively; meanwhile, the discharge energies of EPE film after PD 2h is 4.2774×10^6 pJ. And the discharge energies of the overall encapsulant layer of hot-melting POE and EPE on PET backsheet are 1.7907e+08 pJ, 1.6093e+07 pJ. Table 1 exhibits the above results.

Table 1 Effective charge and discharge energy with different discharge time

Samples	PD time	Q_i (pC)	W (pJ)
	0 h	0	0
POE	2 h	3.9957e+03	6.7314e+06
EPE	2 h	3.8074e+03	4.2744e+06
Hot-melting POE/PET	10 h	1.0972e+05	1.7907e+08
Hot-melting POE/PET	10 h	1.0695e+04	1.6093e+07

Obviously, the effective charge and discharge energy are proportional to discharge time. And the discharge energy is closely related to the number of PD pulse signal. As lengthening the duration of applied voltage, the insulating material with micro defect

absorbs more energy, which results from the fracture of chemical bond. The degradation of polymer materials occurs, when the absorbed energy of polymer material is greater than 5 eV [28]. During PD, the size of defects inside POE film is expanded due to the chemical reactions and electron bombardment, which leads to the increase of discharge energy. Eventually, the growth of electrical tree leads to the breakdown of insulating material.

3.2 **Analysis of Infrared and Raman Spectroscopy**

In order to explore the variation of functional group from micro perspective, the infrared spectrum and Raman spectroscopy are carried out. Infrared spectrum is an important technology commonly employed for analysing the microscopic variation of chemical groups.

The infrared spectroscopies of POE, EPE, the overall encapsulant layer of hot-melting POE on PET backsheet, and the overall encapsulant layer of hot-melting EPE on PET backsheet before and after PD are shown in figure 4. Some important bands occurr in the infrared spectroscopies are listed in table 2.

The infrared spectroscopy of the untreated POE film exhibits the typical peaks of polyethylene including C–H symmetric and asymmetric stretching, CH_3 bending, and (CH_2) group rocking vibration [29]. After PD, the intensity of infrared spectroscopy slightly increases with lengthening the PD time.The absorption peak at 1120 cm^{-1} is induced by C-C stretching vibration of methylene in the saturated hydrocarbon backbone. The peak at 1470 cm^{-1} is assigned the CH_2 bending. The peak at 720 cm^{-1} is attributed to methylene rocking vibration of $(CH_2)n$ where n is greater than 4 [30] because of the existence of ethylene in the POE backbone.

The infrared spectroscopy of the untreated EPE film exhibits the characteristic peaks of bending of CH_3 group and stretching of acetate group. It can be noted that the absorption intensity slightly increases, which reflects the occurrence of subtle scission chain induced by the electron bombardment after PD 120 minutes. The absorption peaks at 719 and 1465 cm^{-1} are considered as the rocking vibration of methylene and the bending of methyl EPE film. And the absorption peaks of EPE film at 1020, 1237, 1371 and 1736 cm^{-1} are attributed to the stretching of C-O, the stretching of CO(=O), the bending of CH_3 group and the stretching of C=O at the EVA layer of EPE films, respectively [21]. The slight reduction of absorbance at the wavenumber of C-O, CO(=O), C=O reflects the slight degradation of EVA layer on the EPE films after PD 120 minutes [31].

According to the IR spectroscopy, it can be found that the hot-melting POE and EPE films exhibit some characteristic peaks at 719, 1463, 2848 and 2916 cm^{-1}, which represents the rocking vibrations, bending, stretching of the methyl (CH_2) in the molecular main chain of POE and EPE. For the hot-melting POE on PET, the infrared peaks at 3206, 1735 and 1414 cm^{-1} are –OH stretching, C=O stretching and C-H bending after PD 10 h, respectively, which is attributed to the generation of H radical and the oxygen-containing radicals induced by electron bombardment. For the hot-melting EPE on PET, the wavenumber at 1236 and 1370 cm^{-1} can be find, which is the stretching of CO(=O) and the C-H bending of the methylene group, respectively. After PD 10 h, an addition peak at 1593, 1697 and 3204 cm^{-1} can be observed, which

represents stretching of C=C, vibration of C-C and–OH stretching of molecular main chain. The change reflects the binding of H radical from hot-melting EPE and oxygen-containing radical from crosslinking agent induced by electron bombardment.

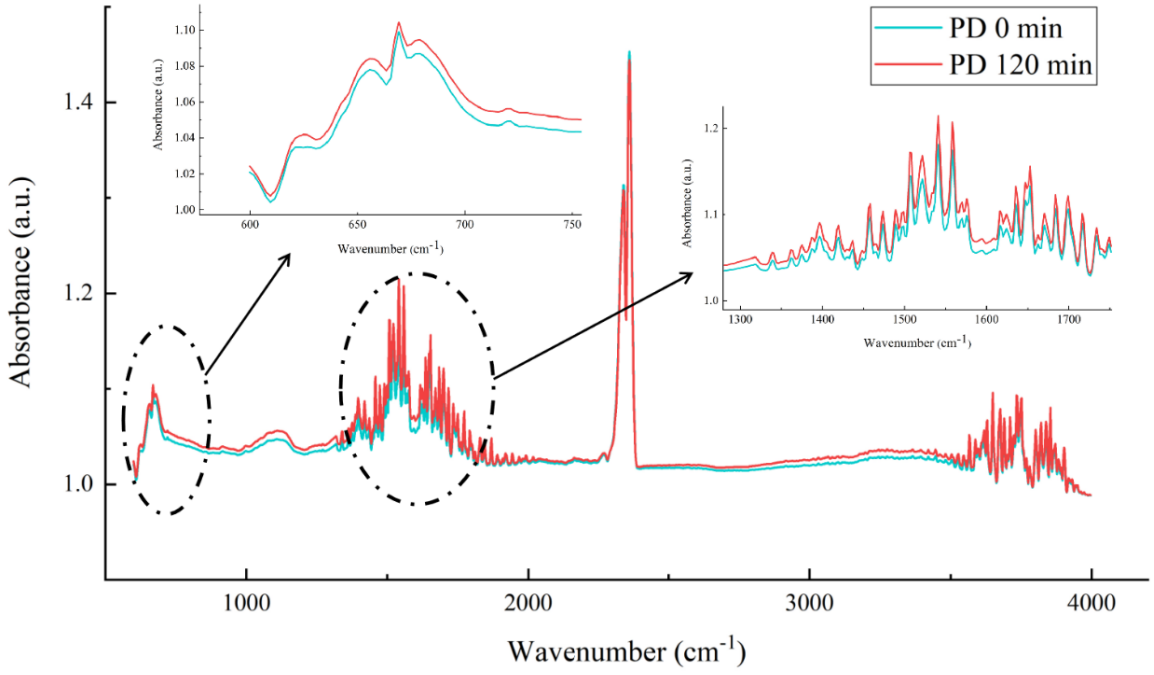

(a)

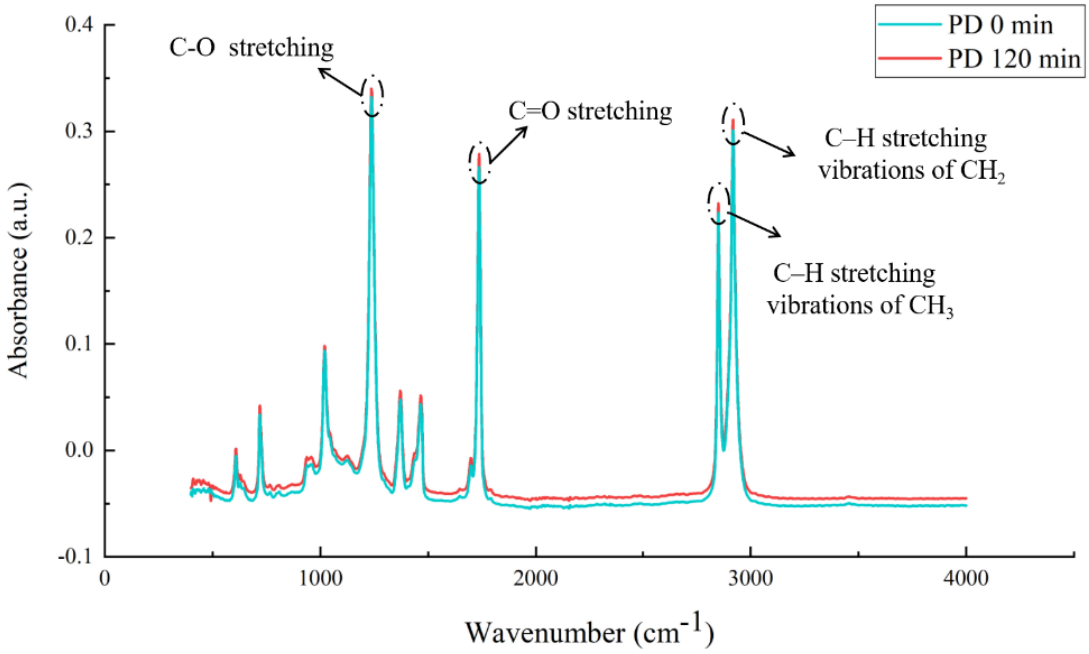

(b)

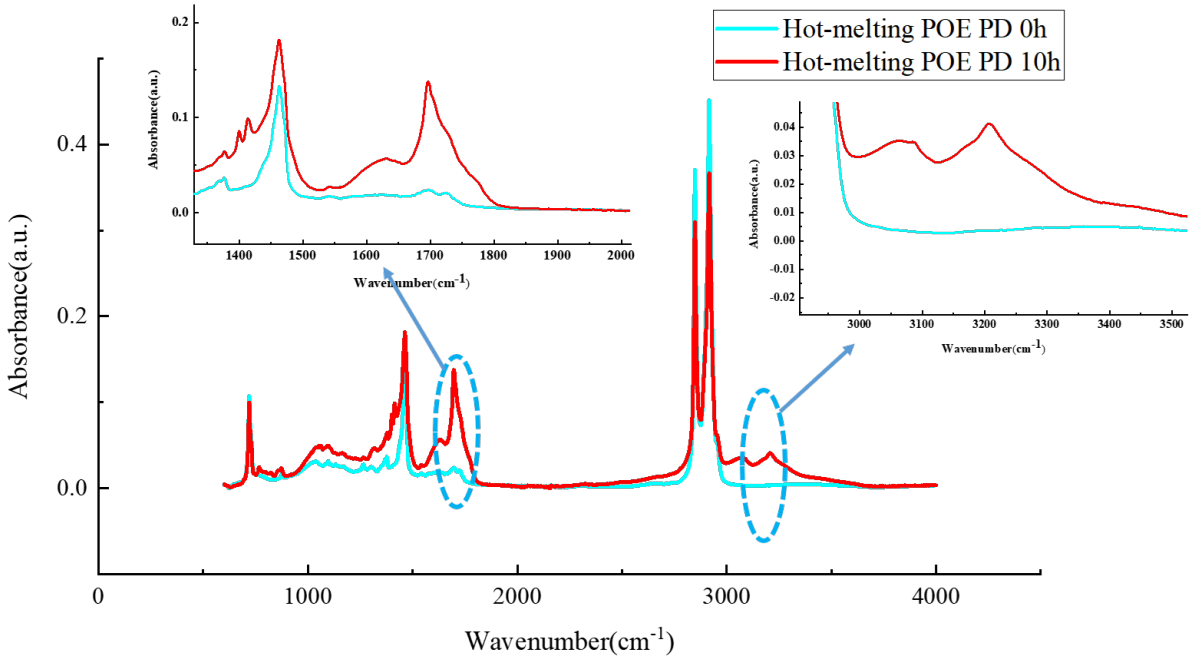

(c)

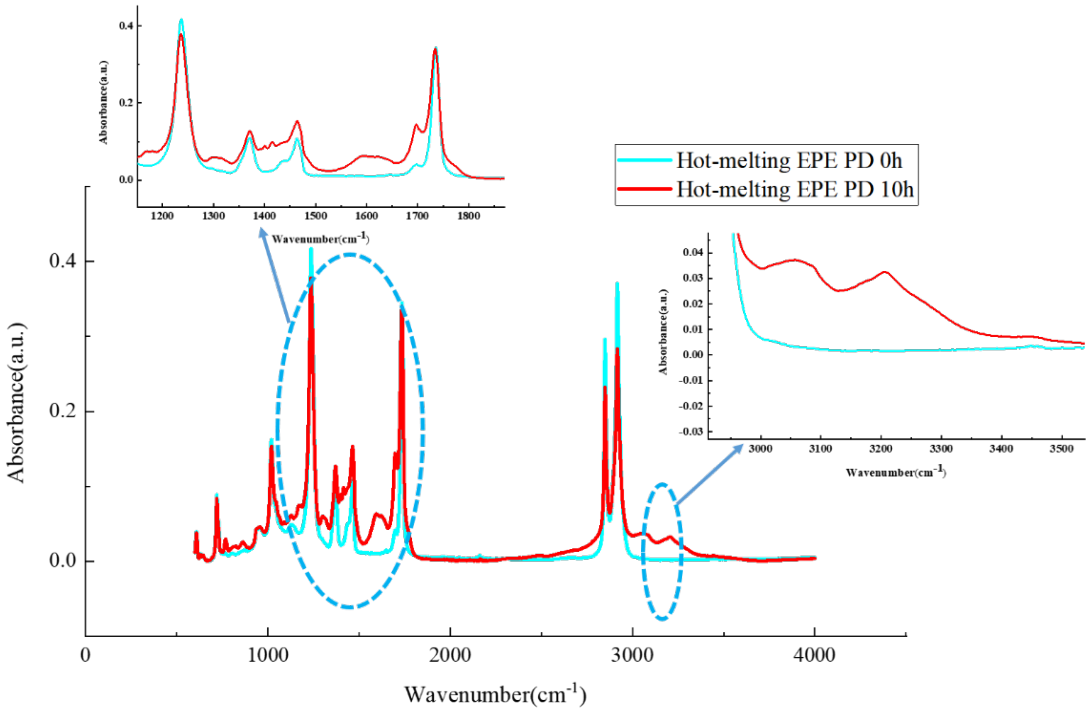

(d)

Figure 4. Infrared spectra of POE (a), EPE (b), hot-melting POE on PET (c) and hot-melting EPE on PET (d).

Table 2 Infrared peak values and their assignments for POE and EPE films

Samples	Wavenumber (cm^{-1})	Assignment
POE	1470	CH_2 bending
	1120	C-C stretching vibration
	720	CH_2 synergistic vibration
EPE	1020	C-O stretching
	1237	CO(=O) stretching
	1371	CH_3 bending
Hot-melting POE	2850 and 2920	C-H stretching
	1414	C-H bending
	1735	C=O stretching
	3206	–OH stretching
Hot-melting EPE	1593	C=C stretching
	1697	C-C vibration
	3204	–OH stretching

Raman spectroscopy of POE film, EPE film, the overall encapsulant layer of hot-melting POE on PET backsheet and the overall encapsulant layer of hot-melting EPE on PET backsheet before and after PD are shown in figure 5. It is obviously that the intensity of Raman peaks increases after being subjected to PD-stressed. The Raman shifts used to reveal the variation of chemical groups in POE adhesive film are listed in table 3. The elevated Raman peaks could be attributed to the structure modification of the POE adhesive film induced by PD. Based on the figure 5, there are relatively intense Raman peaks between the wavenumber of 1000 to 1500 cm^{-1}, which are explained by ethylene unit in the backbone of POE film. The Raman shift at 780, 1295 and 1438 cm^{-1} could be explained by the C–H bending and C–H stretching vibration [32]. The Raman peaks at 1068 and 1126 cm^{-1} are explained by C–C vibration of POE backbone. As for EPE films, besides the Raman peaks consistent with the POE, the Raman peaks at 631, 1724 cm^{-1} reflect the characteristic peaks of EPE films, which are O-C-O bending vibration and C=O stretching vibration, respectively. Specifically, the Raman shifts at 1068, 1297 and 1440 cm^{-1} are attributed to C-C asymmetric vibration, ethylene CH_2 twisting, ethylene and acetate CH_2 bending. Additionally, the Raman shifts from 2800 cm^{-1} to 2920 cm^{-1} could be attributed to the C–H stretching vibration. The intensity of Raman peaks slightly increases with the increase of PD time, which could confirm the subtle degradation of EPE film after PD 120 minutes.

In addition, the hot-melting POE and EPE films on PET backsheet exhibit characteristic peaks at 2850 cm^{-1}, which is mainly attributed to the molecular main chain of polyethylene. Compared with the Raman spectroscopy of POE and EPE films, the Raman intensity of hot-melting POE and EPE films evidently decrease, which is mainly attributed to the $–CH_2$ symmetrical vibration of the molecular main chain induced by the thermal decomposition during hot-melting process. After PD for 10 h, the Raman intensity of hot-melting POE film at 2850 cm^{-1} in the overall encapsulant layer slightly decreases, and the Raman intensity of hot-melting EPE film has almost no change. In addition, the peak at 780, 1322 and 1466 cm^{-1} represents the C-H bonds of molecular main chain. For the POE film, the C=C band at 859 cm^{-1} occurs in the

Raman spectra of hot-melting POE, which could be attributed to the thermal decomposition and electron bombardment in the branched chain of POE. For the EPE film, the O-C-O band at 631 cm^{-1} and C=O band at 1724 cm^{-1} don't occur in the Raman spectra of hot-melting EPE film, which could reflect the decomposition of crosslinking agent during hot-melting process and PD.

Table 3 Raman shifts (cm^{-1}) assignment for POE and EPE [33,34]

Samples	Raman shift (cm^{-1})	Assignment
POE	780	C-H bending
	1295	Ethylene CH_2 twisting
	1438	Ethylene and acetate CH_2 bending
	631	O-C-O bending vibration
EPE	1297	Ethylene CH_2 twisting
	1440	Ethylene and acetate CH_2 bending
	1724	C=O stretching
	2800, 2881 and 2920	C-H stretching
Hot-melting POE	859	C=C band
	1322and 1466	C-H bending
Hot-melting EPE	1068	C-C stretching
	1126	C-C asymmetric vibration

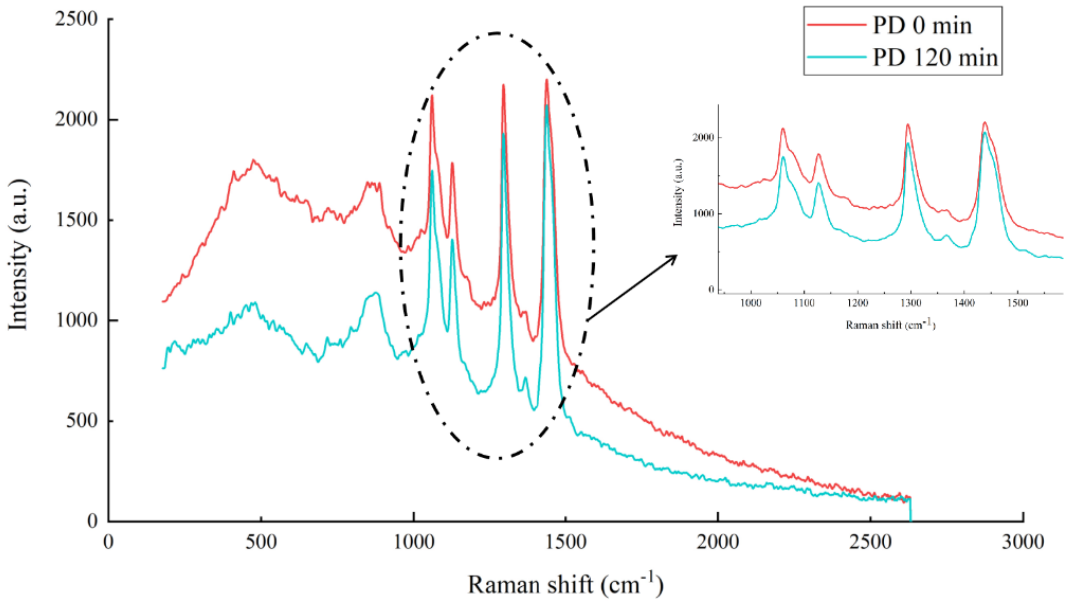

(a)

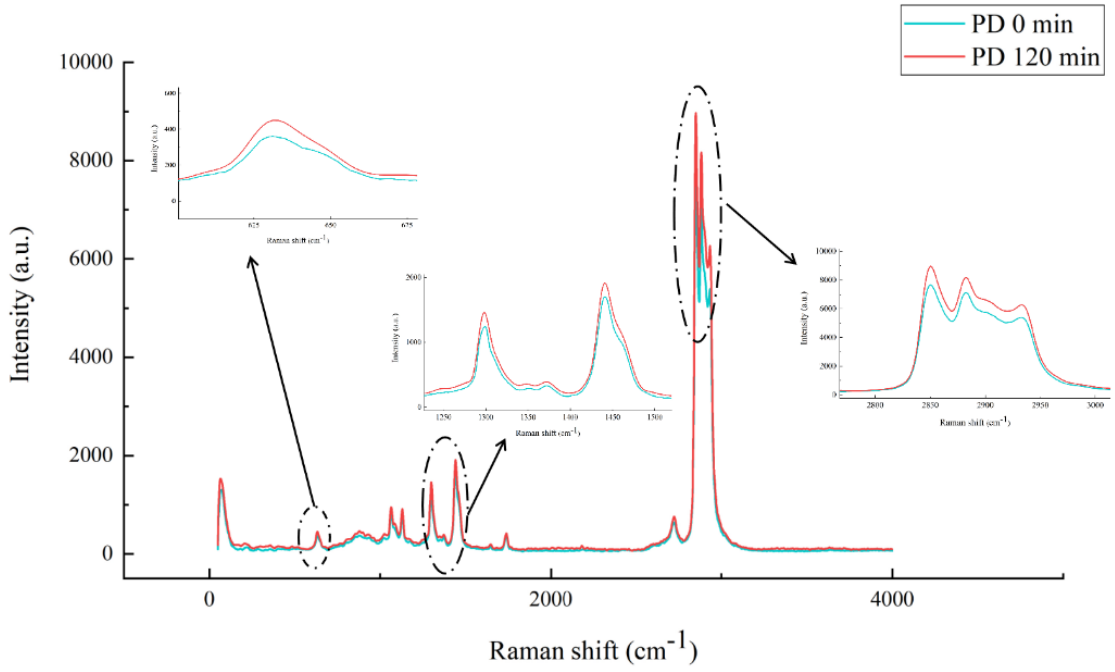
PD 0 min
PD 120 min
Intensity (a.u.)
Raman shift (cm-1)

(b)

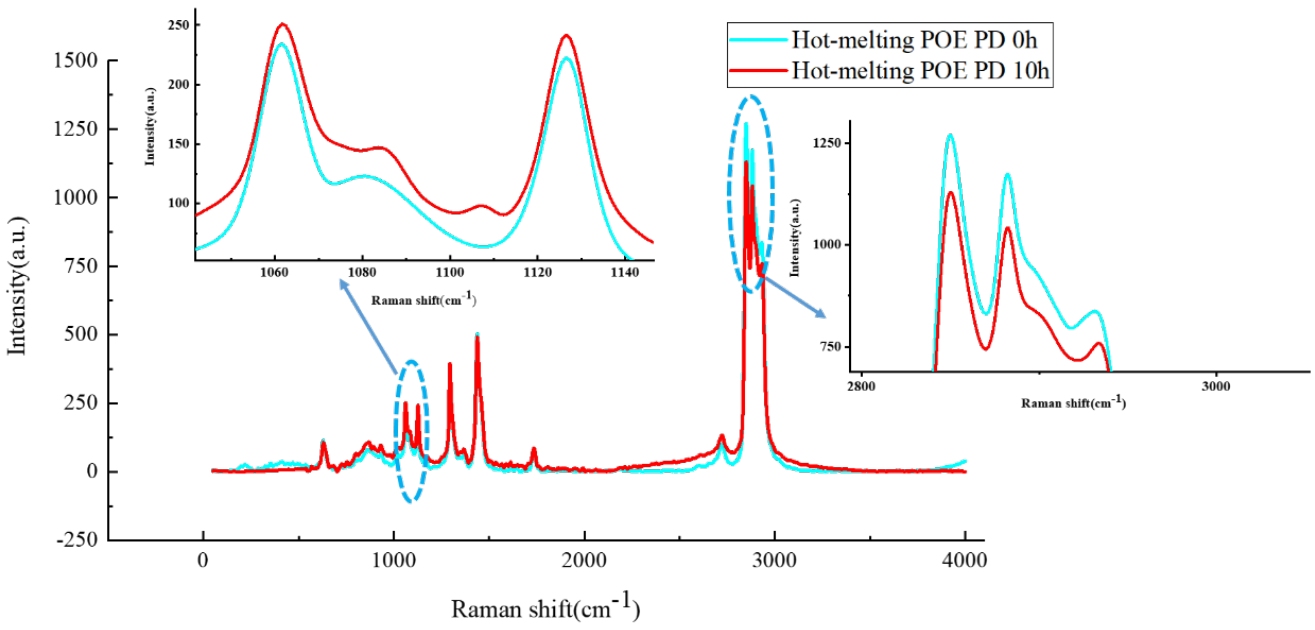
Hot-melting POE PD 0h
Hot-melting POE PD 10h
Intensity(a.u.)
Raman shift(cm-1)

(c)

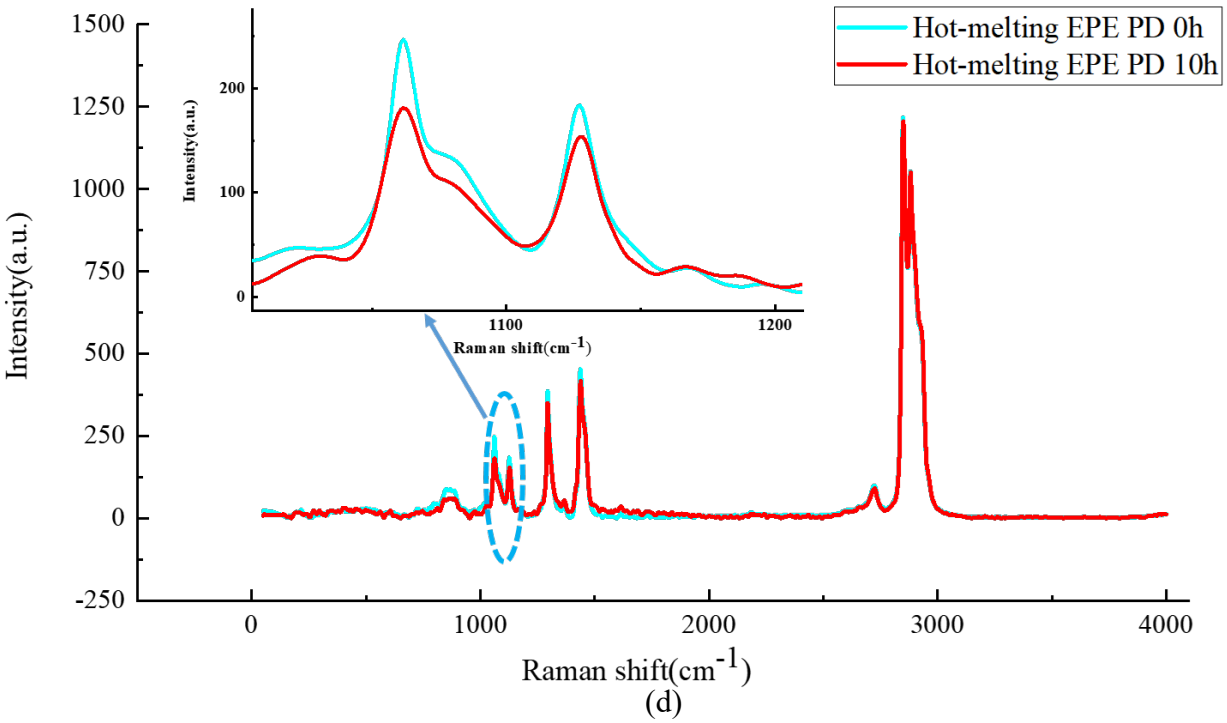

Figure 5. Raman spectra of POE (a), EPE (b), hot-melting POE on PET (c) and hot-melting EPE on PET (d).

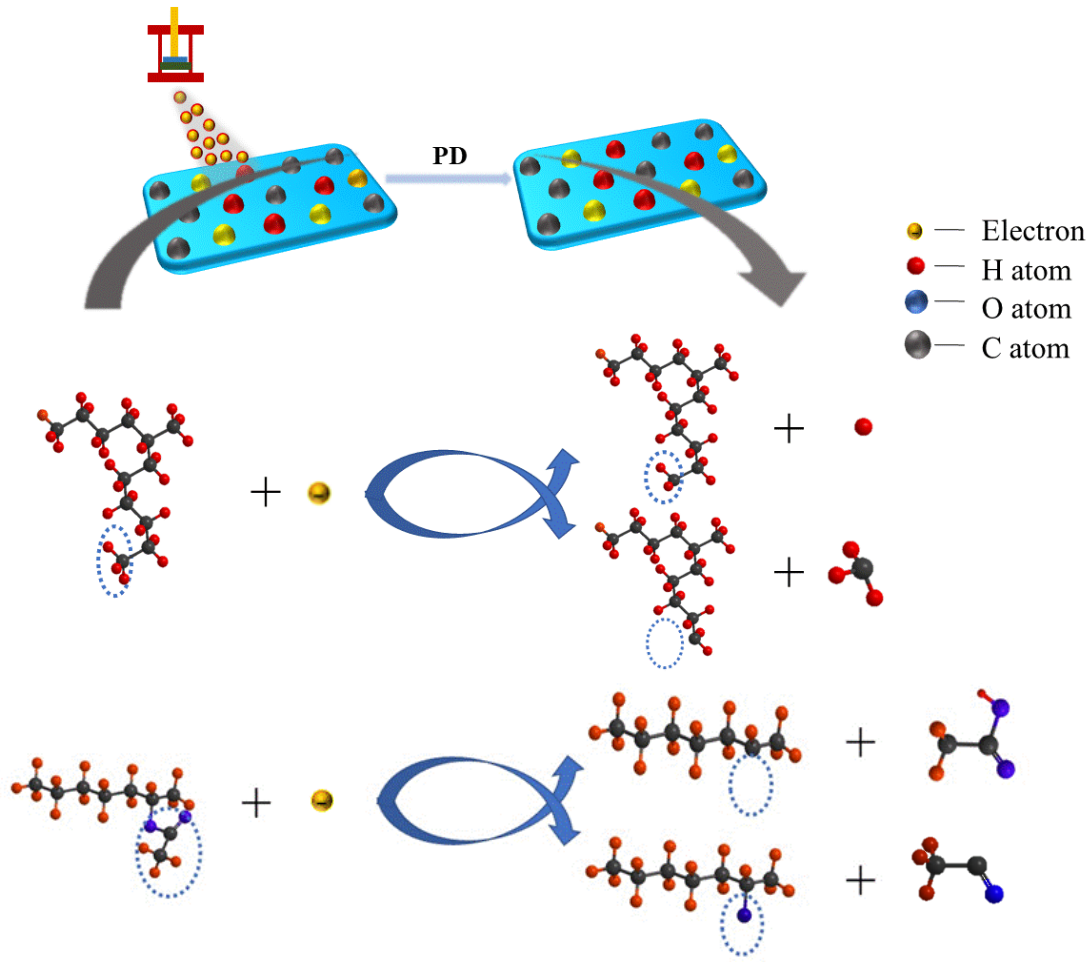

Figure 6. Molecular bond breaking of POE adhesive film under electrical field

From molecular perspective, during partial discharge, the air (O^2) was broke down due to the electron bombardment, which could result in the generation of strong oxidants such as $O\cdot$, O^3 and so on [35,36]. With lengthening the PD time, a large number of strong oxidants could lead to the scission chain of C-H and C-C, which could lead to the degradation of POE film. Meanwhile, when the applied electrical field strength exceeds the critical field strength, the C-C bond and C-H bond at the end of the molecular chain will be broken to form H radicals, CH_3 radicals and CH_2-COOH radicals. Under the action of external electric field, H atom free radicals could attack C and H atoms on the main chain of polymer film, which results in the generation and accumulation of new free radicals. The possible reaction mechanisms were shown in figure 6. The accumulation of free radicals can lead to the generation of space charge, which can cause uneven distribution of field strength around the molecular chain, resulting in the chemical degradation and erosion of polymer [35-37]. Two H radicals are prone to combine to form H_2 molecule, one H radical and one CH_3 radical are easy to combine to form CH_4, and one H radical is prone to combine with CH_2-COOH radical to form CH_3COOH, as well as the C radical is easy to combine to form simple substance C and the like. With the continuous development of PD, when free radical, gas and elemental C expand outward along the molecular gap, electrical tree aging is formed, which could further result in the breakdown of polymer insulating material.

3.3 DSC measurement

The aging phenomenon of polymer insulating material could be characterized by differential scanning calorimetry (DSC) [38]. In order to analyze the temperature characteristics after PD, the DSC measurement of POE adhesive films was performed in a temperature range of 0-200 ℃ with the heating rate of 10 ℃/min. Transition and melting temperatures are commonly parameters for evaluating the temperature characteristics. According to the figure 7, the crystallization and melting curves are above and below curves, respectively. The melting peaks of the POE are between 40 ℃ and 60 ℃ with the peak temperature of 51.99 ℃ and 51.25 ℃ for the untreated POE and the POE after PD 120 minutes; meanwhile, the melting peaks of the EPE exhibit double melting peaks, which are induced by the EVA-POE-EVA structure of EPE film. The melting temperatures (T_m) of EPE are between 40 ℃ and 80 ℃ with the peak temperatures of 48.22 ℃, 71.55 ℃ and 47.85 ℃, 73.63 ℃ for the untreated EPE and the EPE after PD 120 minutes. The crystallization peak temperature (T_c) of POE and EPE films are from 58.86 ℃ to 59.65 ℃ and from 44.24 ℃ to 43.58 ℃ after electron bombardment, respectively. During heating, two small exothermic peak can be noted, which could result from the curing of EVA and POE in the process of heating. After PD 120 minutes, the area of melting peaks are slightly increased, and the position of the melting peaks slightly shifts to the left, which could be attributed to the inferior crystallinity of ethylene induced by the electron bombardment at the main chain of polymer structure; meanwhile, the curing area of EPE film slightly increases after PD 120 min. Additionally, it can be noted that the melting enthalpy are 8.268 J/g, 9.648 J/g and 26.25 J/g, 31.14 J/g for POE and EPE respectively, and the crystallization enthalpy slightly decreases. Based on the figure 7, the melting enthalpy ΔH could be calculated

by integrating the melting peak, and crystallization X_c can be obtained as following formula [39].

$$X_c = \Delta H / \Delta H_0 \times 100\% \quad (3)$$

Where ΔH_0 is the melting enthalpy of POE film fully crystallized. Because the POE and EPE films are copolymer based on polyethylene, the ΔH_0 is 287.3 J/g [39].

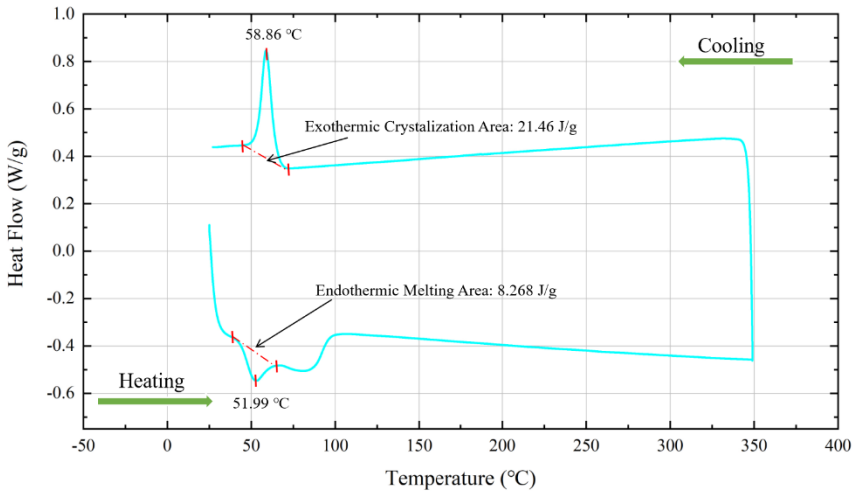

(a)

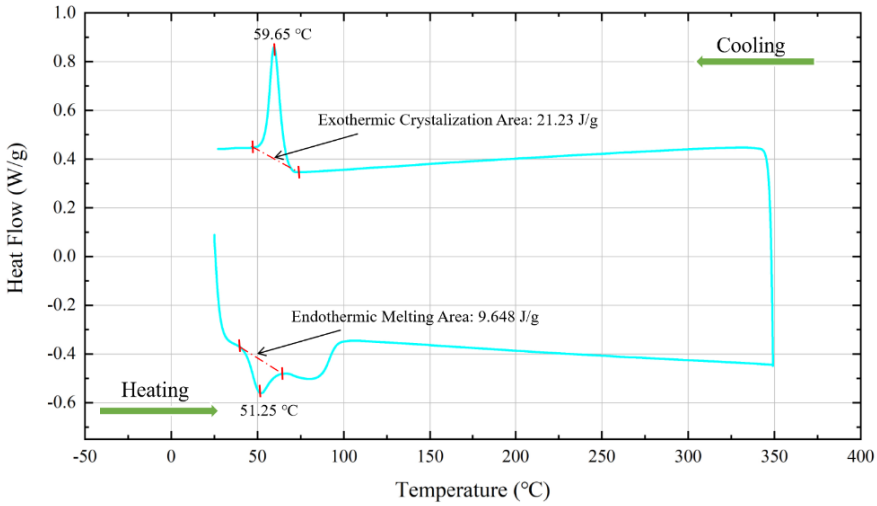

(b)

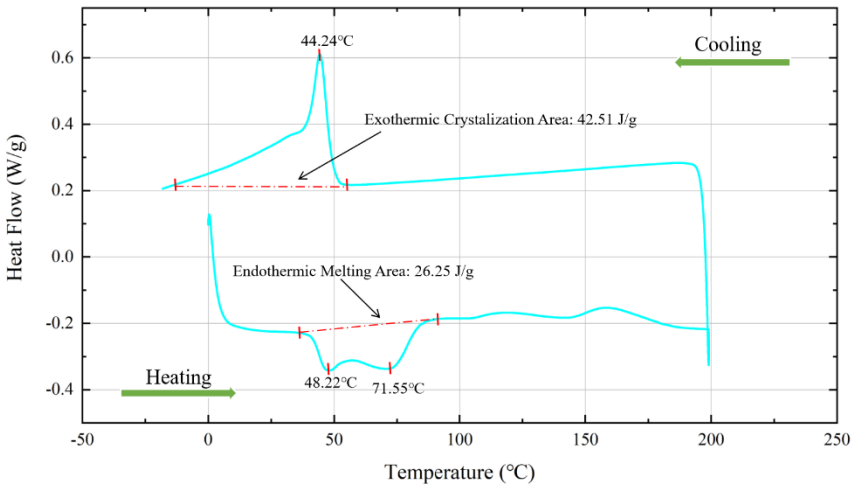
44.24°C
Cooling
Exothermic Crystalization Area: 42.51 J/g
Endothermic Melting Area: 26.25 J/g
Heating
48.22°C
71.55°C
Heat Flow (W/g)
Temperature (°C)

(c)

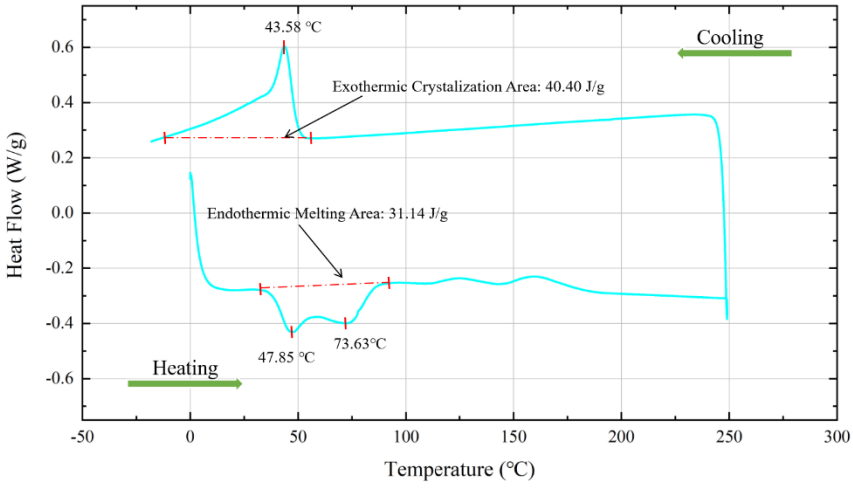
43.58 °C
Cooling
Exothermic Crystalization Area: 40.40 J/g
Endothermic Melting Area: 31.14 J/g
47.85 °C
73.63°C
Heating
Heat Flow (W/g)
Temperature (°C)

(d)

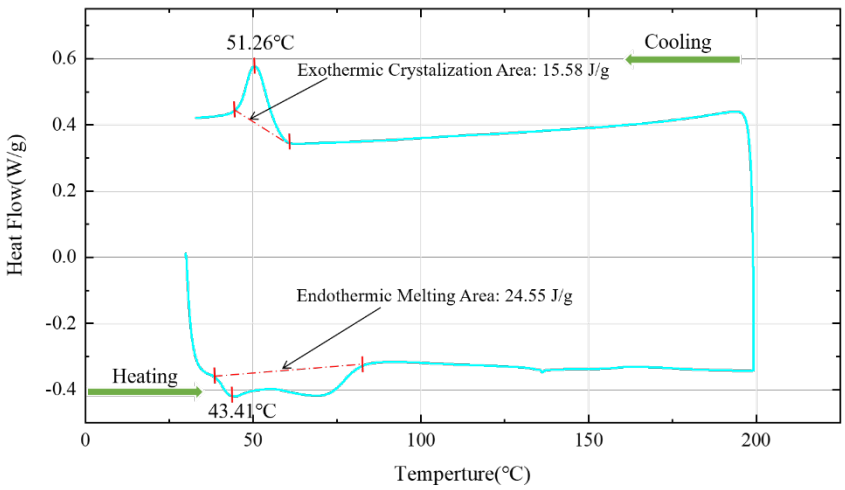
51.26°C
Cooling
Exothermic Crystalization Area: 15.58 J/g
Endothermic Melting Area: 24.55 J/g
Heating
43.41°C
Heat Flow(W/g)
Temperture(°C)

(e)

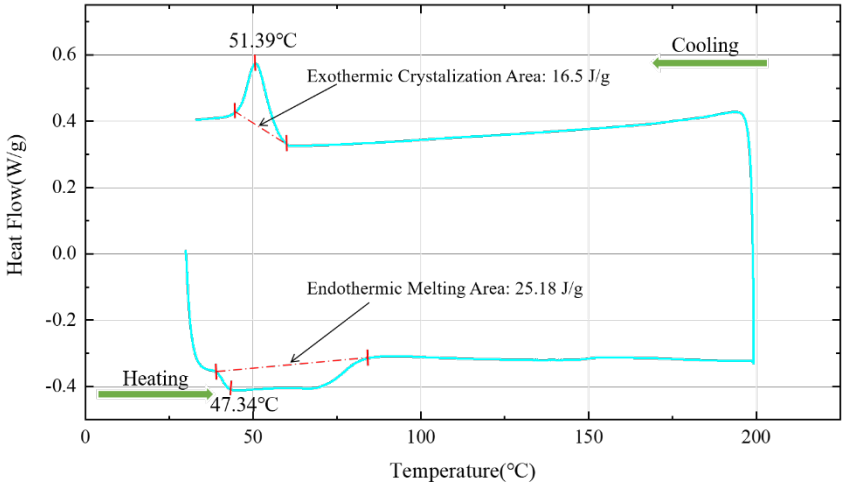
51.39℃
Cooling
Exothermic Crystalization Area: 16.5 J/g
Endothermic Melting Area: 25.18 J/g
Heating
47.34℃
Heat Flow(W/g)
Temperature(℃)
0.6
0.4
0.2
0.0
-0.2
-0.4
0
50
100
150
200

(f)

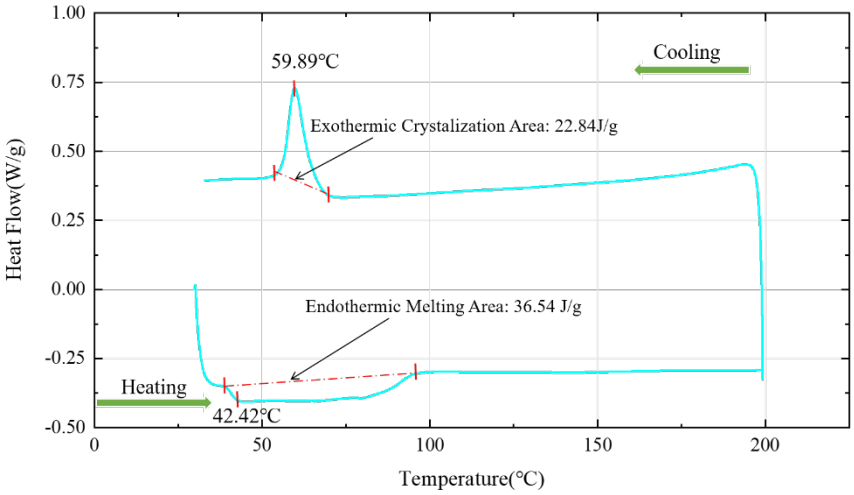
59.89℃
Cooling
Exothermic Crystalization Area: 22.84J/g
Endothermic Melting Area: 36.54 J/g
Heating
42.42℃
Heat Flow(W/g)
Temperature(℃)
1.00
0.75
0.50
0.25
0.00
-0.25
-0.50
0
50
100
150
200

(g)

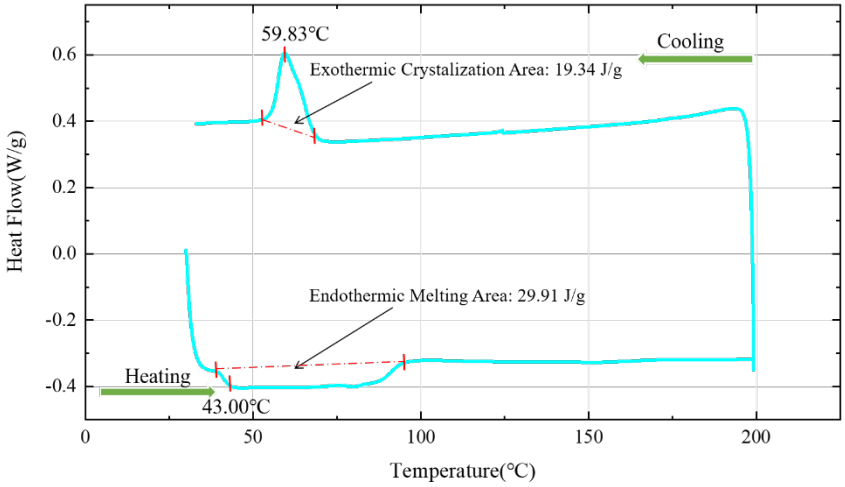

(h)

Figure 7. DSC curve of the untreated POE (a), POE PD 120 min (b), untreated EPE (c), EPE PD 120 min (d), hot-melting POE/PET (e), hot-melting POE/PET PD 10 h (f), hot-melting EPE/PET (g) and hot-melting EPE/PET PD 10 h (h).

According to the Eq. (3), the crystallization X_c is proportional to the melting enthalpy ΔH. Specifically, the crystallizations X_c of POE film are 3.0% and 3.5% before and after PD 120 minutes; at the same time, the crystallizations X_c of EPE film are 6.3% and 6.6% before and after PD 120 minutes. As shown in table 4, it can be noted that the crystallinity of POE and EPE films slightly increase after PD 120 minutes, which could be explained by the shorter PD treatment. For the hot-melting adhesive films of the overall encapsulant layer, the T_m of hot-melting POE and EPE on PET are shifted from 43.14 ℃ to 47.34 ℃ and 43 ℃ to 42.42 ℃, respectively. And the T_c of hot-melting POE and POE on PET are shifted from 51.26 ℃ to 51.39 ℃ and 59.83 ℃ to 59.89 ℃, respectively. In addition, the melting enthalpy of hot-melting POE and EPE on PET are 24.55 J/g and 25.18 J/g, 29.91 J/g and 36.54 J/g, and the crystallizations of hot-melting POE and EPE on PET are shifted from 8.8% to 9% and 10.7% to 13.1% which could be induced by the change of molecular structure result from heating and electron bombardment.

Table 4 Melting and crystallization parameters of samples

Samples	**ΔH (J/g)**	**T_m (℃)**	**X_c (%)**
POE-PD 0 h	8.268	51.99	3.0
POE-PD 2 h	9.648	51.25	3.5
EPE-PD 0 h	26.25	48.22	9.4
EPE-PD 2 h	31.14	47.85	11.2
Hot-melting POE - PD 0 h	24.55	43.41	8.8
Hot-melting POE - PD 10 h	25.18	47.34	9

Hot-melting EPE-PD 0h	29.91	43	10.7
Hot-melting EPE-PD 10g	36.54	42.42	13.1

This change can be attributed to the accumulation of by-products generated by electron bombardment at the defects. In addition, due to the increase in crystallinity of POE adhesive film with different PD time, which increases the mean free path of electrons and the influence of electron bombardment on polymer molecular chains [40]. The electron bombardment could accelerate the growth of electrical tree. Moreover, the increase of crystallinity could result in the accumulation of impurities at defects, which could further decrease the dielectric strength and volume resistance [40,41]. After PD for a long period, the polymer can occur insulating failure and breakdown.

4. Conclusion

Solar energy is considered as the best substitute for mitigating the global energy crisis and greenhouse effect caused by extensively burning of the conventional fossil energy. Therefore, in order to develop advanced PV technology, it is essential to explore the performance of PV modules and find more excellent material for packaging the PV modules. In this paper, the electrical degradation and chemical changes of POE film, EPE film, the overall encapsulant layer of hot-melting POE on PET backsheet and the overall encapsulant layer of hot-melting EPE on PET backsheet are explored from PRPD patterns, infrared and Raman spectroscopies after PD test. Meanwhile, the discharge energy is calculated, which quantitatively reflects the degree of degradation of insulating material. The results from infrared and Raman spectra provide significant support for exploring the degradation from molecular perspective.The calculated results show that the discharge energy raises with lengthening PD duration, which could provide an effective approach for exploring the relationship between the service time of PV system and electrical-induced aging. These results could provide significant reference on developing and designing encapsulant material for PV module in new energy system and deep space exploration.

ACKNOWLEDGEMENTS

This work was supported by the National Natural Science Foundation of China (NSFC) (Grant No. 51877031), the High-level Talents Plan of Shaanxi Province, the State Key Laboratory of Engineering Dielectrics and Its Application (Ministry of Education, China), the State Key Laboratory of Reliability and Intelligence Electrical Equipment (Hebei University of Technology, China, Grant No. EERIKF2018010). The authors acknowledge the help in infrared and Raman spectra measurement professor Xiaojing Chen from Wenzhou University. Meanwhile, the authors appreciate the help in PD measurement with Dr. Peng Wang from Sichuan University and the contribution

in providing the valuable information of PV module in worksite with Liang Wang from Ningxia Panshi Testing & Research Co., Ltd.

REFERENCES

[1] R. Joeri, E. Michel den, H. Niklas, F. Taryn, F. Hanna, W. Harald, S. Roberto, S. Fu, R. Keywan, M. Malte. Paris Agreement climate proposals need a boost to keep warming well below 2°C. Nature. 2016, 534, 631-639.
[2] J. C. Feng, J. Y. Yan, Z. Yu, X. L. Zeng, W. J. Xu. Case study of an industrial park toward zero carbon emission. Appl Energy. 2018, 209, 65-78.
[3] A. Caroline, F. Julia. Path to zero carbon emissions. Science. 2018, 360, 1416-1418.
[4] A. Gholami, M. Ameri, M. Zandi, R. Gavagsaz-Ghoachani, S. Eslami, S. Pierfederici. Photovoltaic potential assessment and dust impacts on photovoltaic systems in Iran: review paper. IEEE J Photovolt. 2020, 10, 824-836.
[5] E. Akrami, A. Gholami, N. Amer, M. Zandi. Integrated an innovative energy system assessment by assisting solar energy for day and night time power generation: Exergetic and Exergo-economic investigation. Energy Convers Manag. 2018, 175, 21-32.
[6] H. Khatib. IEA World Energy Outlook 2011—A comment. Energy Policy. 2012, 48, 737-743.
[7] M. Gagliardi, M. Paggi. Long-term EVA degradation simulation: Climatic zones comparison and possible revision of accelerated tests. Sol. Energy. 2018, 159, 882-897.
[8] B. Adothu, P. Bhatt, S. Chattopadhyay, S. Zele, J. Oderkerk, H.-P. Sagar, F.-R. Costa, S. Makkick. Newly developed thermoplastic polyolefin encapsulant–A potential candidate for crystalline silicon photovoltaic modules encapsulation. Sol Energy. 2019, 194, 581-588.
[9] F. Liu, L. Jiang, S. Y. Yang. Ultra-violet degradation behavior of polymeric backsheets for photovoltaic modules. Sol Energy. 2014, 108, 88-100.
[10] J. W. Zhang, D. K. Cao, S Diaham, X Zhang, X. Q. Yin, Q. Wang. Research on potential induced degradation (PID) of polymeric backsheet in PV modules after salt-mist exposure. Sol Energy. 2019, 188, 475-482.
[11] Y. L. Luo, Z. H. Li, H. Wang. A Review of Online Partial Discharge Measurement of Large Generators. Energies. 2017, 10, 1694.
[12] M. Farahani, H. Borsi, E. Gockenbach, M. Kaufhold. Partial discharge and dissipation factor behavior of model insulating systems for high voltage rotating machines under different stresses. IEEE Electr Insul Mag. 2005, 21, 5-19.
[13] A. Morlier, M. Köntges, S. Blankemeyer, I. Kunze. Contact-free determination of ethylene vinyl acetate crosslinking in PV modules with fluorescence emission. Energy Procedia. 2014, 55:348-355.
[14] N. H. Phillips, B Givot, G Korba, J Loyd, B. O'Brien. Analytical Techniques Used to Determine Chemical Degradation of Polymeric Materials Used in PV Modules after Sustained Exposure to Partial Discharge Voltages. Photovoltaic Specialists Conference. 2012.
[15] J. W. Zhang, D. K. Cao, X. Q. Yin, C. Putson, P. Xiao, Q. Wang. Investigation on

the Effect of Accumulated Charge-Induced Degradation on Multilayer Photovoltaic Insulating Backsheets Based on Atomic Force Microscopy. ACS Appl Energy Mater. 2020, 3, 8946-8952.
[16] C. Hirschl, M. Biebl-Rydlo, M. DeBiasio, W. Mühleisen, L. Neumaier, W. Scherf, G. Oreski, G. Eder, B. Chernev, W. Schwab, M. Kraft. Determining the degree of crosslinking of ethylene vinyl acetate photovoltaic module encapsulants—a Comparative Study. Sol. Energy Mater. Sol. Cells. 2013, 116, 203-218.
[17] M. Ghaffarian Niasar, N. Taylor, P. Janus, X. Wang, H. Edin, R. Clemence Kiiza. Partial discharges in a cavity embedded in oil-impregnated paper: effect of electrical and thermal aging. IEEE Trans Dielect Elect Insul. 2015, 22, 1071-1079.
[18] L. Niemeyer. A generalized approach to partial discharge modeling. IEEE Trans Dielect Elect Insul. (1995, 2, 510-528.
[19] A. Cavallini, F. Ciani, G. Mazzanti, G. C. Montanari. First electron availability and partial discharge generation in insulation cavities: effect of light irradiation. IEEE Trans Dielect Elect Insul. 2005, 12, 387-394.
[20] R. J. Van Brunt. Stochastic Properties of Partial-discharge Phenomena. IEEE Trans Dielect Elect Insul. 1991, 26, 902-948
[21] H. Lllias, G. Chen, P. L. Lewin. Partial discharge behavior within a spherical cavity in a solid dielectric material as a function of frequency and amplitude of the applied voltage. IEEE Trans Dielect Elect Insul. 2011,18, 432-443.
[22] J. W. Zhang, D. K. Cao, Y. C. Cui, F. Wang, C. Putson, C. Song, Influence of potential induced degradation phenomena on electrical insulating backsheet in photovoltaic modules. J Clean Prod. 2019,208, 333-339.
[23] B. Fruth, L. Niemeyer. The importance of statistical characteristics of partial discharge data. IEEE Trans Dielect Elect Insul. 2002,27, 60-69.
[24] F. Gutfleisch, L. Niemeyer. Measurement and simulation of PD in epoxy voids. IEEE Trans Dielect Elect Insul. 1995, 2, 729-743.
[25] R. Bodega, P. H. F. Morshuis, M. Lazzarnol, F. J. Wester. PD recurrence in cavities at different energizing methods. IEEE Trans Instrum Meas. 2004, 53, 251-258.
[26] E. Lemke. A Critical Review of Partial Discharge Models. IEEE Electr Insul Mag. 2012, 28, 11-16.
[27] Z. D. Wang, X. Wang, X. Yi, S. T. Li, J. V. Hinshaw. Gas Generation in Natural Ester and Mineral Oil Under Partial Discharge and Sparking Faults. IEEE Electr Insul Mag. 2013, 29, 62-70.
[28] C. Y. Li, J Hu, C. J. Lin, B. Y. Zhang, G. X. Zhang, J. L. He. Fluorine gas treatment improves surface degradation inhibiting property of alumina filled epoxy composite. AIP Advances. 2016, 6, 25017.
[29] G. Oreski, A. Omazic, G. C. Eder, Y. Voronko, L. Neumaier, W. Mühleisen, C. Hirschl, G. Uvari, R. Ebner, M. Edler. Properties and degradation behaviour of polyolefin encapsulants for photovoltaic modules. Prog Photovoltaics. 2020, 28, 1277-1288.
[30] S. Mitra, A. Ghanbari-Siahkali, P. Kingshott, S. Hvilsted, K. Almdal. An investigation on changes in chemical properties of pure ethylene-propylene-diene rubber in aqueous acidic environment. Mater Chem Phys. 2006, 98, 248-255.

[31] Y. X. Wang, C. X. Chen, X. Wu, Z. H. Wang, S. M. Wen, J. Yu, C. H. Yan, W. Cong. Improved antibiofouling properties of photobioreactor with amphiphilic sulfobetaine copolymer coatings. Prog. Org. Coat. 2020, 144, 105666.
[32] C. Peike, T. Kaltenbach, M. Koehl, K. Weiß. Non-destructive degradation analysis of encapsulants in PV modules by Raman Spectroscopy. Sol Energy Mater Sol Cells. 2011, 95, 1686-1693.
[33] B. S. Chernev, C. Hirschl, G.-C. Eder. Non-Destructive Determination of Ethylene Vinyl Acetate Cross-Linking in Photovoltaic (PV) Modules by Raman Spectroscopy. Appl. Spectrosc. 2013, 67, 1296-1301.
[34] C. C. Lin, P. J. Krommenhoek, S. S. Watson, X. H. Gu. Depth profiling of degradation of multilayer photovoltaic backsheets after accelerated laboratory weathering: Cross-sectional Raman imaging Sol. Energy Mater. Sol. Cells. 2016, 144:289-299.
[35] R. J. Van Brunt. Physics and chemistry of partial discharge and corona - recent advances and future challenges. IEEE Trans Dielect Elect Insul.1994, 1, 761-784.
[36] N. H. Phillips, B. Givot, B. O'Brien, L. C. Hardy, J. Loyd, W. Schoeppel, C. Jaeger, C. Humpert, R. Schumacher, C. Knoll. Study of partial discharge effects of PV backsheet component films. Structure property relationships, and measurement consistency. 2011 37th IEEE Photovoltaic Specialists Conference. 2011, 003609.
[37] D. Adhikari, D. M. Hepburn, B. G. Stewart. Comparison of partial discharge characteristics and degradation in several polymeric insulators. IET Sci. Meas. Technol. 2012, 6, 474-484.
[38] C. Capitain, J. Ross-Jones, S. Möhring, N. Tippkötter. Different scanning calorimetry for quantification of polymer biodegradability in compost. International Biodeterioration & Biodegradation. 2020, 149:104914.
[39] X. Zhu, J. D. Wu, Y. L. Wang, Y. Yin. Characteristics of partial discharge and AC electrical tree in XLPE and MgO/XLPE nanocomposites. IEEE Trans Dielect Elect Insul. 2020,27(2):450-458. [42] Y. Tanaka, N. Ohnuma, K. Katsunami, Y. Ohki. Effects of crystallinity and electron mean-free-path on dielectric strength of low density polyethylene. IEEE Trans Dielect Elect Insul. 1991,26(2):258-265.
[340] Y. Tanaka, N. Ohnuma, K. Katsunami, Y. Ohki. Effects of crystallinity and electron mean-free-path on dielectric strength of low density polyethylene. IEEE Trans Dielect Elect Insul. 1991,26(2):258-265.
[41] S. N. Kolesov. The influence of morphology on the electric strength of polymer insulating. IEEE Trans Dielect Elect Insul. 1980,15(5):382-388.